Mapping the spatial distribution of geomorphological processes in the Okstindan area of northern Norway, using Geomorphic Process Units as derived from remote sensing and ground survey

STEPHEN D. GURNEY AND ANNETT BARTSCH

Gurney, Stephen D. & Annett Bartsch (2005). Mapping the spatial distribution of geomorphological processes in the Okstindan area of northern Norway, using Geomorphic Process Units as derived from remote sensing and ground survey. *Fennia* 183: 1, pp. 1–14. Helsinki. ISSN 0015-0010.

The delineation of Geomorphic Process Units (GPUs) aims to quantify past, current and future geomorphological processes and the sediment flux associated with them. Five GPUs have been identified for the Okstindan area of northern Norway and these were derived from the combination of Landsat satellite imagery (TM and ETM+) with stereo aerial photographs (used to construct a Digital Elevation Model) and ground survey. The Okstindan study area is sub-arctic and mountainous and is dominated by glacial and periglacial processes. The GPUs exclude the glacial system (some 37% of the study area) and hence they are focussed upon periglacial and colluvial processes. The identified GPUs are: 1. solifluction and rill erosion; 2. talus creep, slope wash and rill erosion; 3. accumulation of debris by rock and boulder fall; 4. rockwalls; and 5. stable ground with dissolved transport. The GPUs have been applied to a 'test site' within the study area in order to illustrate their potential for mapping the spatial distribution of geomorphological processes. The test site within the study area is a catchment which is representative of the range of geomorphological processes identified.

Stephen D. Gurney, Department of Geography, The University of Reading, PO Box 227, Whiteknights, Reading RG6 6AB, UK. E-mail: s.d.gurney@reading.ac.uk.
Annett Bartsch, Institute of Photogrammetry and Remote Sensing, Vienna University of Technology, Gusshausstrasse 27–29, A-1040 Vienna, Austria. E-mail: ab@ipf.tuwien.ac.at. *MS received 26 January 2005.*

Introduction

The creation of a semi-automated system for the mapping of geomorphological processes which utilises data from remote sensing and produces output through a Geographical Information System (GIS) has long been an ideal within geomorphology. Despite major advances in both remote sensing and GIS in recent decades, however, for most areas of the world it is far from being realised. An intermediate step would appear to be the identification of geomorphic signatures related to process domains (e.g. Giles 1998) or Geomorphic Process Units (GPUs, see Gude et al. 2002) using a mixture of spatial data from both remote sensing and ground survey, with all the data being stored and queried in a GIS. The geomorphological processes that will be identified by such techniques will clearly vary from region to region and will, in part, be determined by climate, terrain etc.

The present paper documents an attempt to map the spatial distribution of geomorphological processes in a sub-arctic, mountainous environment dominated by glacial and periglacial processes using remotely sensed data and field survey. The concept is essentially that of Gude et al. (2002), who identified the GPUs as representing areas with homogenous process composition. In order to quantify processes, the GPUs must be able to identify erosion, transportation and deposition of sediments.

The Okstindan area was chosen for this study since much geomorphological mapping has already been undertaken here using traditional

means (e.g. Harris 1982) and because it contained a site (the Rabotsbekken catchment) that could be readily compared with the Kärkevagge catchment of northern Sweden where Bartsch et al. (2002) have already investigated sediment transport processes using the 'GPU approach'.

A further aim of this investigation was to gain additional knowledge about the spatial extent and importance of non-glacial mass movements (largely solifluction) in the Rabotsbekken test site of the study area, both at present and during the Holocene. Okstindan has seen several investigations of solifluction over the last three decades (e.g. Harris 1973, 1981; Elliott & Worsley 1999) and a continuation of this work using recently developed techniques was believed to be worthwhile.

Study area

The mountainous Okstindan area is located in the Norwegian section of the Scandinavian mountain range some 50 km south of the arctic circle and 70 km to the east of the Atlantic Ocean (Fig. 1). It borders Sweden in the east and belongs to the Hemnes district of Nordland county. The area investigated comprises the immediate surroundings of the Okstindan ice cap, its outlets and flanking glaciers. The glaciers and perennial snowfields cover an area of approximately 58 km^2 as calculated from Landsat 7 ETM+ imagery acquired in September 1999. The ice cap has two major outlet glaciers, Vestre Okstindbreen and Austre Okstindbreen (Knudsen & Haakensen 1998). The highest summits in the area are Oksskolten (1916 m) and Okshornet (1901 m) which are located just east of the ice cap. The study area itself ranges from ca. 650 to 1000 m a.s.l.

Geologically, the study area belongs to the Caledonides fold-belt (Strand & Kulling 1972). The bedrock consists mostly of mica-schists locally rich in garnet, but phyllite, quartzites, hornblende schists, marble and granites are also present. The sedimentary rocks of the area lie within the Rødingsfjall nappe (Rutland & Nicholson 1965) and are part of the Cambro-Silurian group within the Scandinavian pre-Devonian Caledonides (Holtedahl 1960).

During the Weichselian, the whole area was covered by inland ice with Oksskolten forming a nunatak. Currently till covers most areas outside the Neoglacial maximum of the glaciers. Evidence from erratics, striations, roches moutonnées and eskers indicate that ice movement was mainly from the southeast to the northwest (cf. Blake & Olsen 1999). Deglaciation occurred at about the same time as in Beiarn to the north at ca. 9300 years BP (see Andersen 1975). The extent of the

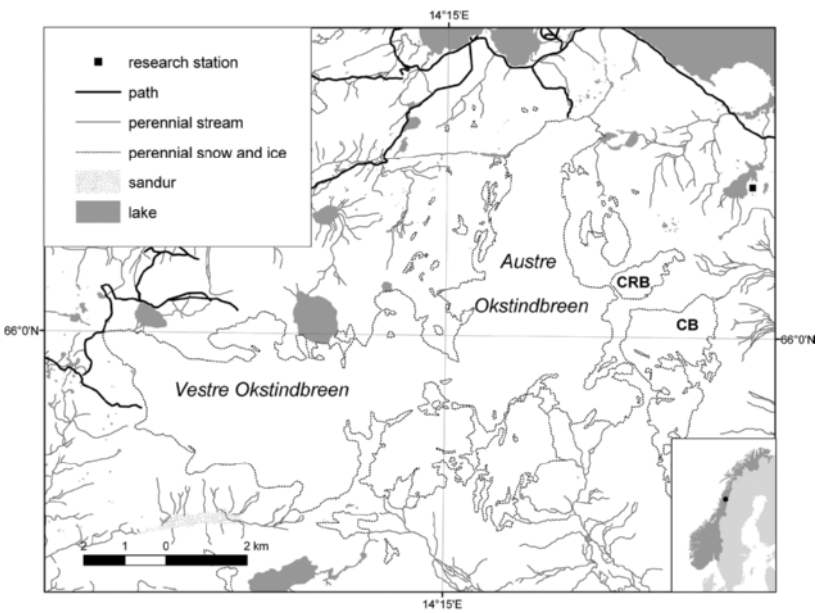

Fig. 1. Main features of the Okstindan study area and its location within Norway. Glaciers referred to in the text labelled CRB (Charles Rabot-breen) and CB (Corneliussen-breen).

local glaciers has varied during the Holocene, and the Neoglacial maximum was achieved in the Little Ice Age (1550–1850 AD) at a date in the mid-18th century (Winkler 2003). The Little Ice Age limits are generally around 1 to 2 km in front of the current glacier positions (Griffey & Worsley 1978). Currently the outlet glaciers of the Okstindan ice cap are in retreat along with all of the flanking cirque glaciers, with the exception of Corneliussen-breen, which has advanced by about 100 m since the early 1970s (Knudsen & Theakstone 1997).

In the absence of a permanent meteorological station in the immediate vicinity, climatological parameters need to be extrapolated from the nearest meteorological station at Hattfjelldal (ca. 50 km to the SSW). Harris (1982) estimated a mean annual air temperature (MAAT) of 0°C at about 700 m a.s.l., whilst Hall (1985) estimated that the MAAT is –2 to –4 °C. Annual precipitation is around 1500 mm, with snow cover at 180 d yr^{-1}. Winter snow cover thickness varies between almost none to over 10 m (Gurney & Lawrence 2004) due to redistribution by the wind. The dominant wind direction is believed to be from the SW (Raben et al. 2000).

The MAAT value indicates that the region is within the area of sporadic permafrost (as defined by King 1986) and on the outer edge of the discontinuous permafrost zone for Scandinavia (Etzelmüller et al. 1998). Nevertheless, only isolated patches of perennially frozen ground have been observed (through excavations in successive years), these in locations which show special micro-topographic properties, like exposure to wind e.g. the crests of moraine ridges (Griffey & Worsley 1978). The surficial cover of till consists of a frost susceptible, silty, sand matrix with larger clasts, and patterned ground phenomena are commonly developed within it. These comprise of non-sorted polygons and circles (including earth hummocks or thufur), sorted circles and solifluction lobes on slopes (Harris 1982).

The study area is characterized by arctic-alpine vegetation (Körner 1999), and the growing season is very short. Four vegetation zones related to altitude (sub-, low, mid- and high alpine belt) occur. The sub-alpine belt is a transition zone from closed montane forest to the treeless alpine belts where the upper limit corresponds to the current treeline at about 660 m a.s.l. The major tree species in this zone at Okstindan is *Betula pubescens* ssp. *tortuosa* (Ellis & Ellis 1978). The low alpine belt represents the upper limit for the occurrence of *Vaccinium myrtillus*. Within the mid-alpine belt, heath vegetation (*Ericaceae*, grasses and sedges) disappears (Ellis & Ellis 1978). In the surroundings of glaciers and at higher altitudes only a few pioneer species can be found. This is defined as the high-alpine zone. The extent of the Neoglacial zone, which has no vegetation cover, is variable due to glacier advance and retreat.

Methodology

Initially, a database was created from existing maps and remotely sensed data. These spatial data were processed to produce first order information on cover type and therefore likely geomorphological process. A Digital Elevation Model (DEM) was then created and used to orthorectify the satellite imagery and create additional parameters such as terrain (slope angle and aspect) and topology (the relationships between the process areas from a sediment transport point of view). The results from satellite image analysis and stereo-photogrammetric processing were then combined with the results of the field measurements and observations. Finally, process group layers were produced and from these, possible process combinations were identified. It was from these possible process combinations that the GPUs were finally formulated. Further explanation is given for each of the stages.

Data sources and spatial data processing

The available spatial data included paper maps, aerial photographs, and satellite imagery (Table 1). Of most importance in the process were the aerial photographs and the satellite imagery. Nevertheless, several topographic and geological maps of the region by Statens Kartverk (Norway) and NGU (Geological Survey of Norway) are available at a scale of 1:50,000 and these were scanned and some elements of interest, such as the glacier extent and hydrology, were digitised. When using a variety of spatial data sources the problem of differing projections and datums must be overcome. During the second half of the last century, three different models have been in use (Mugnier 1999): the NGO 1948 (Oslo Observatory Datum), European Datum 1950 and WGS84. All co-ordinates were converted to WGS84 to enable overlays.

Other paper maps used included a geological map (Reynolds 1978) and a vegetation map (Ellis & Ellis 1978) which related to the NE sector on the study area only. The lack of Ground Control Points (GCPs) meant that the georeferencing accuracy of these maps was less than 50 m. Nevertheless, they formed a useful adjunct to the field survey data.

Due to the cloudy and largely snow covered nature of the area, suitable Landsat satellite imagery were available for 1984 (Landsat 5 TM) and 1999 (Landsat 7 ETM+) only. Both images contain information on land cover for the same season when snow coverage is largely limited to the glaciated areas. The Landsat 7 image has the benefit of a panchromatic band (Band 8) with 15 m x 15 m resolution.

Distortions and spectral discrepancies within remotely sensed data from mountainous areas are mainly caused by altitude differences, relief orientation concerning the sensor position and illumination effects. In order to combine different spatial data sets and extract new information, it is necessary to remove or minimize any distortions using data provided by a DEM – a process known as orthorectification. The resolution of the elevation data must be higher than those of the remotely sensed data, which it is intended to correct. In this case the Landsat scenes obtained had a pixel spacing of approximately 30 m. The source for the elevation data are aerial photographs, which were scanned with a pixel spacing of 1 m. Since the available maps for georeferencing have a scale of 1:50,000 and the equidistance of the elevation lines is 20 m, the maximum resolution of the final DEM is not less than 20 m x 20 m and could therefore be used for orthorectification of the satellite imagery. The generation of the DEM used is discussed later.

The two Landsat images were pre-processed using the orthorectification algorithm provided by Erdas Imagine software. The photogrammetrically derived DEM was used as additional input for the orthorectification. GCPs were collected using map co-ordinates which were transformed first to WGS84 where necessary. These UTM x, y coordinate pairs were complemented by their associated altitude in metres a.s.l.

A landcover classification was created and this was used in part to delimit the entire extent of the glaciers. The chosen approach utilised the Maximum Likelihood method. A non-topographic normalized image (with no correction of illumination effects) was used as input in order to capture all snow covered areas, including those in shadow. Contrary to other landcover types, snow and ice can be identified in shadows and under varying illumination. A further reason for not applying a normalization procedure in this case was that the available algorithm would exclude shadow areas which actually account for much of the snow and ice covered terrain. The resulting classes comprise snow and ice (including areas in shadow), shadow over other landcover types, non-vegetated areas, vegetated regions and water. Misclassifications resulting from differing illumination in landcover types other than snow and ice do not effect the further analyses since this information is not used other than as an illustration (Fig. 2) and errors were

Table 1. Spatial data sources utilised in the study.

Data source	Projection/Media	Comments
Topographic Map 1:50,000 sheet 2027 III, 1986	UTM, WGS84	Georeferenced in ArcINFO™
Topographic Maps 1:50,000 sheets 1927 II, 1926 I, 2026 IV, 1984–1986	UTM, European Datum 1950	Georeferenced and transformed in ArcINFO™
Flight Record Co-ordinates	NGO 1948	Transformed in ENVI
Aerial Photographs 1:30,000 acquired 31–08–1998	Black & White Diapositives (CD-ROM once scanned)	11 images scanned at 750 dpi
Landsat 5 TM acquired 30–08–1984	CD-ROM	Level 1R (full coverage)
Landsat 7 ETM+ acquired 07–09–1999	CD-ROM	Level 1R (full coverage)
Landsat 7 ETM+ acquired 07–09–1998	CD-ROM	Level 1 (part coverage)

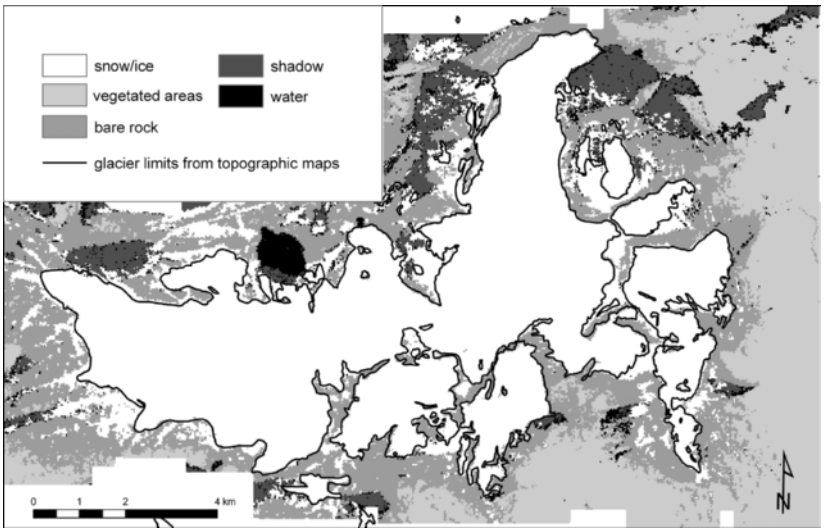

Fig. 2. Landcover classification of Landsat 5 TM, 1984. Glacier outlines from 1:50,000 topographic maps.

not assessed. The Landsat 5 image from 1984 was chosen for the classification, since it was acquired at the end of the ablation season and shows minimal snow coverage. All bands were used except the thermal band (Band 6). Classification accuracy was assessed through comparison with the orthophotographs (from 1998) which were acquired at roughly the same time of year and at the same time of day as the Landsat image. 150 randomly distributed points were used for the assessment and perennial snow and ice fields showed satisfactory results, as did bare areas and vegetation, although some water surfaces were classified incorrectly. Nevertheless, the overall classification accuracy for the reclassified image was 86.49% and this was considered sufficient. Ultimately, shaded snow and ice areas could be successfully separated from other shaded regions and landcover classes including vegetated area, bare rock and water.

A Normalised Difference Vegetation Index (NDVI) was extracted from the Landsat 7 ETM+ scene, which was acquired during the growing season. NDVI values increase as vegetation cover increases and hence it is a very useful tool in mapping. Creating NDVI from ETM+ data involves the use of Band 3 (Red, 0.63–0.69 μm) and Band 4 (Near Infrared, 0.78–0.90 μm), in the form NDVI = (Band 4 – Band 3)/(Band 4 + Band 3). Such a ratio accounts for most of the illumination effects, since they are equal in all bands. To ensure that all influence is removed, however, a topographic normalisation was applied before ratioing. The calculated values within the area of the DEM range from –0.68 to 0.56 with the highest values observed within the low and subalpine vegetation zone and the lowest values observed within the Okstindan ice cap. Indeed the large area of the ice cap results in a low average NDVI for the entire study area of –0.08.

DEM creation

Eleven aerial photographs were available for the study area. These were acquired on two different tracks on 31 August, 1998 by Fjellanger Widerøe Kart AS with an RMK Top 15. Only areas with an overlap of 60% are suitable for the extraction of elevation data of sufficient accuracy, which meant that the overlap between tracks (at only 30%), could not be processed in combination with the within track data. In addition to limitations of coverage, the following problems caused errors in the DEM extraction: shadow areas, continuous high albedo (low image content) of snow over large areas and clouds, including the shadows they cast. Locations affected by such phenomena were post-processed.

The aerial photographs were scanned (at 750 dpi) and then the elevation data was extracted using the Orthomax module in Erdas. Regions of the DEM with anomalies (sinks and peaks) were identified and then post processed through either recalculation using different parameters (see Gooch

et al. 1999) or substitution with other elevation information. The first solution is only applicable in the case of artefacts, which are the result of low image content. Ultimately it was not possible to remove all errors, which confirms the analysis undertaken by Fox and Gooch (2001) who were also unable to overcome the problem presented by large areas of featureless snow. An alternative is the use of slightly underexposed colour infra-red photographs (Fox & Nuttall 1997), which improves the snow surface texture. Such photographs, however, were not available for the current research.

The final DEM was imported into ArcINFO. The single images had missing or inaccurate information removed and were combined using the MOSAIC function, which allows the combination of images with continuous data like elevation models, which overlap each other. Abrupt changes along boundaries were prevented through the use of a weighted average method. The georeferenced topographic maps were used to replace any missing information.

An accuracy assessment of the DEM was undertaken employing ground-based height measurements obtained using a hand-held GPS receiver and a digital altimeter (68 points) and spot heights gathered from the topographic maps (85 points). The final DEM covers an area of ca. 157 km^2 and the elevation ranges from 527 m to 1924 m ASL. This exceeds the known maximum altitude of 1916 m at Oksskolten and is probably caused by interpolation errors caused by the pronounced peak-shape of this mountain. Those areas requiring post-processing totalled 6.2 km^2, which represents only 4% of the entire DEM and these were mostly confined to glaciated terrain.

Field data collection

The primary aim of the fieldwork, which was conducted in July/August 2001 and 2002, was to create a database of data points which could be used in the formulation of the GPUs. A secondary aim was the verification of some of the existing mapping. Some 79 data points were obtained in the study area, grouped into three areas around the Okstindan ice cap (Fig. 3). Area I represents the north eastern sector of the Okstindan area, Area II is located west of the snout of Austre Okstindbreen and Area III is just north of the snout of Vestre Okstindbreen. The data points selected in these areas were chosen to represent both recently geomorphically active and inactive sites. Since the glacial environment is and has been dominant, features such as moraines and glacier forelands are present. Table 2 lists all site types together with their data point frequency. This classification of sites refers to landform and geomorphic activity. The category 'slope without other geomorphic fea-

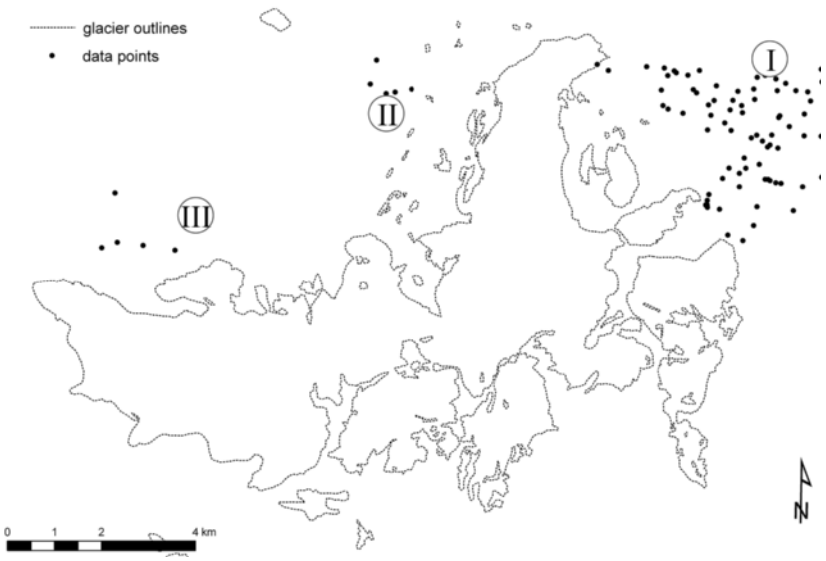

Fig. 3. Location of the 79 field data points used to verify the image interpretation and GIS analysis.

Table 2. Cover types at the 79 data points obtained during fieldwork for verification of the image interpretation and GIS analysis.

Cover types	Number of sites
Bedrock	7
Bog	5
Braided river	2
Glacio-fluvial deposits	3
Gletschervorfeld (glacier foreland)	3
Earth hummocks (thufur)	3
Inactive talus slope	4
Moraine	5
Nivation – surrounding of perennial snowpatch	2
Non-sorted circles and polygons	10
Ridge	5
Slope without other geomorphic features	12
Solifluction slope	15
Talus slope (active)	2
Valley floor (below treeline)	1
Total	79

tures' comprises currently geomorphically inactive sites but those which might have witnessed slope processes at some stage since deglaciation. The data points of 'inactive talus slopes' have certainly been active within the Holocene, but show no current mass movement features.

In active areas, such as 'nivation' (sites in the immediate vicinity of perennial snow patches), 'solifluction slope' and 'talus slope (active)', a range of sediment transport processes take place. Wash denudation was not observed directly, but was assumed to take place in areas with low vegetation coverage and an inclined ground surface. Patterned ground as a feature of frost heave, has not been included in this list since material is generally not moved away by the processes responsible. Fine material produced by frost action processes, however, might be subsequently relocated by wash denudation. Therefore, wash denudation was mapped on inclined areas showing patterned ground. Exposed patterned ground on top of ridges is subject to deflation. Indeed, this process might even be causative for the formation of patterned ground in such locations (Harris 1982). The rockfall areas are located between Charles Rabot-breen and Corneliussen-breen below a free face (for glacier location see Fig. 1).

Table 3 indicates those process types investigated specifically for sediment transport and relationship to vegetation zones. In order to analyse the relationship between vegetation parameters and sediment transport processes, the dominant plant species at each site were identified and total vegetation coverage estimated. The number of mapped sites within the high alpine zone is smaller than that of the low and mid-alpine zones due to limited accessibility in the field. Nevertheless, it is apparent that solifluction is confined to the low and mid-alpine vegetation zone. Wash denudation on the other hand occurs within all zones.

GPS measurements were taken at all 79 sites using a Garmin Etrex handheld GPS receiver to determine exact locations in combination with satellite data, and these were also used in the accuracy assessment of the DEM.

Formulation of the GPUs

The sources for the parameterisation for the GPU formulation were the processed Landsat data (30 m x 30 m resolution), the DEM (20 m x 20 m resolution) and the field measurements and observations. Regolith type (from maps and field survey) and topology (from the DEM) were introduced as

Table 3. Process types investigated specifically for assessing sediment transport and their relationship to vegetation zones.

Process type	Frequency	Vegetation Alpine zone			
		Sub	Low	Mid	High
Solifluction	16	0	12	4	0
Talus creep only	6	0	0	4	2
Wash denudation	33	1	19	8	5
Seasonal flooding	3	0	1	1	1
Earth slides	2	0	2	0	0
Deflation	3	0	3	0	0
Rockfall	2	0	0	1	1
Nivation	3	0	0	1	1

additional parameters at the final stage. Topology defines the relationship between objects, with the objects in this case being the process areas, which are connected to each other from the viewpoint of sediment input and output. All parameters of relevance are listed in Table 4. Once all the data had been processed it was then combined to create four process group layers. A simple decision tree classification using expert-knowledge based on the literature and on the field observations has been applied. Each resulting layer contains process features (source or deposition) with equal parameter specifications (Table 5). When these groups are combined, five unique process combinations are possible which represent the GPUs at the study site. The final GPUs derived (Table 6) have a spatial resolution of 30 m x 30 m, the same as the Landsat data which served as input.

Table 4. Parameter groups and the information that they have been based upon.

Parameter group	Information contained
Terrain	Slope angle, Curvature, Aspect Absolute altitude Relative altitude (height of objects such as rockwalls) Direction of flow
Landcover	Regolith type (boulders, fine debris) Presence/absence of vegetation NDVI value Presence/absence of perennial snow or ice
Topology	Relation to neighbouring zone (such as potential source area) e.g. above or below Horizontal distance

Table 5. Parameters for the sediment transport groups.

Process group	Parameter group	Specification
1	Terrain Landcover	11° to 21° slope angle, lower limit elevation 660 m 0.2 to 0.45 NDVI, firn fields excluded
2	Terrain Landcover	21° to 40° slope angle –0.2 to 0.2 NDVI, firn fields excluded
3	Terrain Landcover Topology	21° to 40° slope angle –0.2 to 0.2 NDVI below rockwalls (i.e. directly adjacent to source area)
4	Terrain Landcover	>40° slope angle no vegetation, firn fields excluded

Table 6. GPU classification scheme. Total area and percentages given are for the Rabotsbekken catchment (test site) of the study area. Note perennial snow and ice covers ca. 40% of the catchment.

GPU	Description	Area (km^2 [%])
1	Solifluction and rill erosion. Found on moderate slopes and rill erosion often occurs between lobes.	0.68 [6.9]
2	Talus creep (as defined by Rapp 1960), slope wash and rill erosion. Found mostly below rockwalls on debris covered slopes and freeze-thaw processes are probably involved.	0.63 [6.4]
3	Accumulation of debris by rock and boulder fall on talus slopes characterized by creep, slope wash and rill erosion, mud and debris flow. Similar to GPU 2 except these areas lie below their source areas, the rockwalls and disturbance by sediment input is high (so no vegetation cover or pioneer plants only).	0.30 [3.0]
4	Rockwalls, source area for debris for rock and boulder fall. The source area for GPU 3.	0.96 [9.8]
5	Stable ground with dissolved transport only or a paraglacial environment.	3.35 [34.0]

The parameter groups 'terrain' and 'landcover' were used to identify GPU 1 (solifluction and rill erosion). The slope gradient value is derived by combining field data with the DEM. The DEM values differ from the field data because of their ground resolution. Since the process area extraction is based on the 20 m x 20 m DEM, these values were favoured. The lower limit for the occurrence of solifluction lobes corresponds roughly to the treeline. The calculated minimum and maximum NDVI value for solifluction areas was used as a landcover parameter.

GPUs 2 (talus creep) and 3 (debris accumulation by rock and boulder fall) feature similar parameter values but the latter includes topology as well, because it requires a source area above. Both are confined to slopes between 21° and 40°. The potential source areas for gravity determined mass movements such as pebble fall are expected to show a slope gradient above 40° and little or no vegetation cover.

Once created, GPUs 1, 2 and 3 were evaluated using the field data and all were considered accurate. This data set, however, included only one, albeit extensive, site where active rockfall deposits could be identified which is located between Charles Rabot-breen and Corneliussen-breen (cf. McCarroll et al. 1998). This site was correctly classified by the GPUs, although since no further sites could be identified using the orthophotos, a more thorough evaluation was not possible. Due to limited accessibility, no field data points were obtained for GPU 4 (rockwalls, source area for debris). These areas are, however, clearly visible on the orthophotographs and can be observed from a distance on the ground.

The vegetation coverage estimated during field surveys was compared with the result of the NDVI calculations. A linear relationship between the vegetation coverage estimate and NDVI value was observed (Pearson correlation, $R^2 = 0.795$). The relationship between NDVI values and certain geomorphological cover types is clearly of interest. For example, the NDVI value for areas affected by solifluction is positive in all cases. A similar range of NDVI values was extracted for areas with earth slides and deflation. The latter generally does not show dense plant coverage, but is populated by dwarf *Salix* species and other low growing plants which are typical of exposed ridges. Talus creep (GPU 2) and rockfall deposit sites (GPU 3), however, show low or even negative NDVI values. Compared to the extracted geomorphometric parameters for the different process types, there are considerable differences for the NDVI ranges between processes.

The species composition in solifluction areas (GPU 1) depends on the type of solifluction (stone- or turf-banked lobes). Major components of the vegetation cover are *Betula nana* and *Salix* ssp. Overall coverage exceeds 80% at most sites. Typical sites with solifluction lobes are located within the low alpine belt. Beside mosses and grasses, *Empetrum nigrum* and *Vaccinium myrtillus* are usually found growing on the upper part of the lobes which are better drained.

Slopes with talus creep (GPU 2) experience disturbance of the vegetation cover and are generally located at higher altitudes. The coverage by vascular plants is very low (maximum 7%). A cryptogram crust consisting of lichen and mosses covers the ground (at up to 70%). A low head wall is often situated above scree and the slope itself is mostly covered by debris, which has been delivered by processes such as rockfall. No lobes are developed but downslope movements are expected due to frost creep. This site also represents the upper limit of the mid-alpine vegetation zone. The debris is covered by mosses (at up to 30%) and pioneer vascular plants such as *Ranunculus glacialis*.

Application of the GPUs to the Rabotsbekken 'test site'

Although the whole of Okstindan was used as 'training' area for the formulation of the GPUs, they have only been applied to the test site of Rabotsbekken catchment. This is because GPUs are concerned with sediment transport (and if this idea is extended, they could be used to create a sediment budget) which can only be sensibly considered within a catchment context. The Okstindan area includes many catchments, although these are either small or were not completely covered by the area of the DEM generated. The Rabotsbekken catchment was chosen because it is representative of Okstindan, in that it contains all of the processes and features found in the area as a whole. Rabotsbekken was also amongst those areas of Okstindan which had been documented by previous workers and this meant that verification of the GPUs could be more thorough. In terms of possible comparison with previous work, the Rabotsbekken catchment was large enough (at 10 ha) to be realistically compared with the Kärkevagge

catchment considered by Bartsch et al. (2002), which is about twice this size.

Figs. 4 and 5 provide a 3D DEM and a 3D GPU map for the Rabotsbekken test site. Table 6, which lists the GPUs, also gives the areal extent of each GPU in this area. With the GPU mapping approach it has been possible to assign all areas of the test site, outside of the glacial realm and those areas in deep shadow on the imagery, to a GPU. In this sense the mapping is far more complete than previous work which has tended to be feature specific (e.g. Fig. 4 in Harris 1982). In essence this is the advantage of 'process mapping' as opposed to 'feature' mapping which has been most prevalent in the past.

Advantages and disadvantages of the GPU approach

It can be extremely difficult to compare the results of a GPU type mapping exercise based on remote sensing with those achieved through more traditional means (e.g. Harris 1982). The emphasis in most previous mapping exercises has centred on the identification of geomorphological features, rather than geomorphological processes. It is true, of course, that the presence of features often infers one or more processes. However, it is not always clear whether these processes are necessarily active since many features, once established, can be maintained in the absence of one or more of their

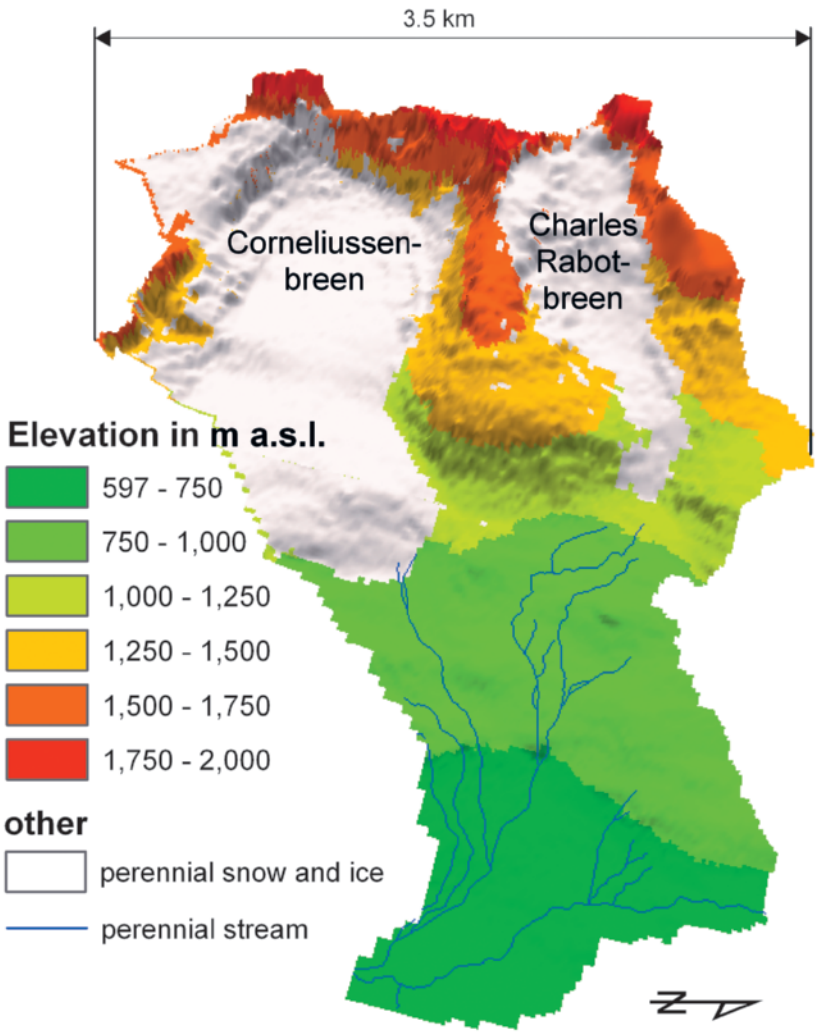

Fig. 4. 3D DEM of the Rabotsbekken test site, z-factor = 1, view direction E to W.

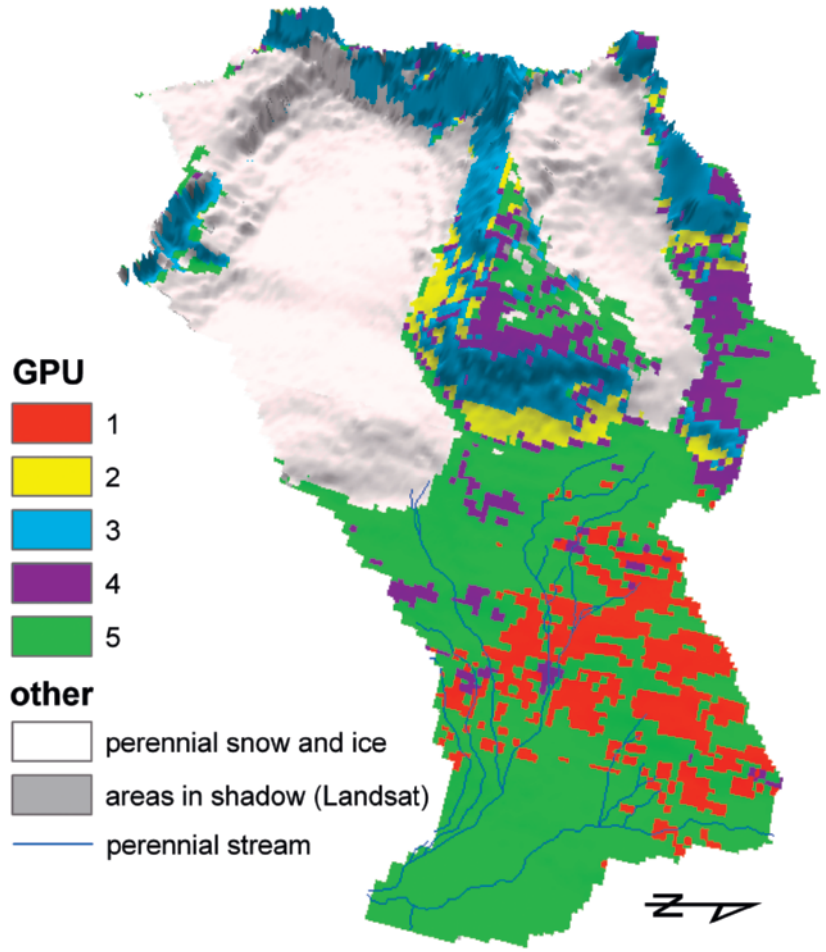

Fig. 5. 3D GPU map of the Rabotsbekken test site, z-factor = 1, view direction E to W. For GPU classification see Table 6.

formative or initiating processes. This is certainly the case with many periglacial features as found in the Okstindan area. Since the current study aimed to map processes and classify all areas, it is by its very nature, more complete than previous mapping exercises. It also enables areas which have not been visited on the ground to be classified whereas previous mapping, even if it had a remote sensing component (such as the use of aerial photographs), necessitated a ground survey. The greater coverage achieved using the GPU approach means that it is an important step closer to modelling sediment transport through the landscape.

Countering these obvious advantages, however, there are some disadvantages. There is clearly a greater problem with the possible mis-classification of areas when using the GPU approach than is the case with the feature specific mapping conducted previously. Also, some geomorphological features are not identified at all, for example, pronival ramparts (cf. Shakesby 1997), although the processes contributing to them are (see later discussion). The labour involved is also not necessarily reduced using the GPU approach over more traditional means, although the processing can be done at any time of year and is not restricted to 'field seasons' (at Okstindan much of the ground is snow covered for the greater portion of the year which is a considerable restriction to fieldwork). That said, since satellite imagery utilising the visible part of the spectrum is required, there is a restricted number of images available for any one year due to cloudiness and/or snow cover.

Of specific interest in this research were the processes of solifluction and the landforms created by them. Both stone-banked and turf-banked

solifluction lobes can be found in the Okstindan area (Harris 1982; Worsley 1993). They are mostly developed in Weichselian till (Harrison & Macklin 1991; Elliott 1996; Elliott & Worsley 1999). Harris (1982) mapped the altitudinal limits of solifluction lobes in the area and reports a wider altitudinal range (660 to ca. 1200 m a.s.l.) than that identified by the current research. The Harris data, however, resulted from very detailed mapping and involved a large number of sites (over 400), many of which were smaller than those that could be used in the current research due to the necessity to combine ground survey with satellite data. Nevertheless, there is in general very good agreement between the data sets.

There are certain features which exist in the area which have not been expressly identified by the GPU mapping of the current research, although the processes which combine to form them largely have. The case of pronival ramparts (formerly termed protalus ramparts, Shakesby 1997) being a good example. It could be argued, however, that a number of features such as this are not easy to identify in the field through direct observation and hence in this respect there is an element of subjectivity in all mapping exercises. The existence of a pronival rampart located on a talus slope between Corneliussen-breen and Charles Rabot-breen has been proposed by Harris (1986). The ridge has a height of 4.75 m, a width of 10 m and a length of 100 m. It consists of mainly angular clasts and boulders, but a finer matrix also appears to have been incorporated. It is assumed that these fines have been deposited in connection with rockfall events. This rampart is considered to be active (Harris 1986). Clearly such features are important in the context of the landscape of Okstindan. It should be noted, however, that GPU 3 essentially encapsulates the processes involved (admittedly with the exception of the role of the perennial snow) and, therefore, from a sediment transport point of view the mapping remains successful.

GPU mapping in the Kärkevagge of northern Sweden (Bartsch et al. 2002), resulted in the formulation of seven GPUs (although one of these was further subdivided into three categories). Okstindan and the Kärkevagge have much in common, in terms of latitude, landscape and climate, and therefore there are considerable similarities between the GPUs for these areas. The main difference in terms of the geomorphological processes identified, however, is that dirty avalanches make a substantial contribution to sediment movement rates in the Kärkevagge and account for two of the assigned GPUs, whereas at Okstindan these phenomena have not been directly identified. Furthermore, GPU types at Kärkevagge are more varied since process areas overlap to a higher degree due to its specific setting and landscape development. Despite the differences between the two sites, however, it can be seen that this geoinformatics based approach to the determination of sediment transport process areas is transferable between these two periglacial mountain environments.

Conclusions

Mapping the spatial distribution of geomorphological processes through the formulation of Geomorphic Process Units (GPUs) is a relatively new approach. In this study it was possible to classify the landscape of the Rabotsbekken test site into one of five categories which together represent all the terrain excluding perennial snow/ice. Whilst there are significant advantages with this approach over more traditional, often feature specific, mapping, the process is based on extensive expert knowledge and is thus only semi-automated. As a procedure it is time-consuming. Further difficulties were encountered due to the nature of the study area which is sub-arctic and mountainous. It has been demonstrated, however, that this approach for GPU derivation is applicable at Okstindan and is thus transferable between mountainous periglacial environments.

This study is based on the interpretation of digital elevation and satellite data at a particular resolution for a specific environment. The layers used for the derivation of the GPUs in the final stage of the process, however, could be replaced by products resulting from a different methodology of process area determination. This would enable the 'GPU approach' to be transferred to other environments and at different scales. This technique could, therefore, be applied in other landscapes and climatic zones, although there is still considerable work to be done before such mapping will become routine.

ACKNOWLEDGEMENTS

The authors would like to thank Dan Butterfield, Vebjørn Hansen, Kjetil Kvitnes and Mikhail Lamakin for field assistance. Tvis Knudsen (University of Aarhus) provided the aerial photograph transparencies. Kevin

White (University of Reading) provided much relevant expertise and experience in the remote sensing operations. Fieldwork in 2001 was funded by a Research Grant from The Royal Society, Dudley Stamp Memorial Fund and a Leonard Sutton Scholarship from The University of Reading. This work was conducted whilst Dr Bartsch was in receipt of a studentship at the Department of Geography, The University of Reading. The assistance of two anonymous referees has improved the text substantially and is greatly appreciated.

REFERENCES

Andersen BG (1975). Glacial geology of northern Nordland, north Norway. *Norges Geologiske Undersøkelse* 320. 74 p.

Bartsch A, M Gude, C Jonasson & D Scherer (2002). Identification of Geomorphic Process Units in Kärkevagge, northern Sweden, by remote sensing and digital terrain analysis. *Geografiska Annaler A* 84, 171–178.

Blake KP & L Olsen (1999). Deglaciation of the Svartisen area, northern Norway, and isolation of a large ice mass in front of the Fennoscandian Ice Sheet. *Norsk Geografisk Tidsskrift* 53, 1–16.

Elliott G (1996). Microfabric evidence for podzolic soil inversion by solifluction processes. *Earth Surface Processes and Landforms* 21, 467–476.

Elliott G & P Worsley (1999). The sedimentology, stratigraphy and ^{14}C dating of a turf-banked solifluction lobe: evidence for Holocene slope instability at Okstindan, northern Norway. *Journal of Quaternary Science* 14, 175–188.

Ellis S & J Ellis (1978). Notes on the vegetation of northeast Okstindan. In Fenwick IM (ed). Okstindan Preliminary Report for 1976, Okstindan Research Project, 57–68. Unpublished report.

Etzelmüller B, I Berthling & JL Sollid (1998). The distribution of permafrost in southern Norway – a GIS approach. In Lewkowicz AG & M Allard (eds). Permafrost, Seventh International Conference, June 23–27, Yellowknife, Canada. *Collection Nordicana* 57, 251–257.

Fox AJ & MJ Gooch (2001). Automatic DEM generation for Antarctic terrain. *Photogrammetric Record* 17: 98, 275–290.

Fox AJ & A-M Nuttall (1997). Photogrammetry as a research tool for glaciology. *Photogrammetric Record* 15: 89, 725–737.

Giles PT (1998). Geomorphological signatures: classification of aggregated slope unit objects from digital elevation and remote sensing data. *Earth Surface Processes and Landforms* 23, 581–594.

Gooch MJ, JH Chandler & M Stojic (1999). Accuracy assessment of digital elevation models generated using the ERDAS Imagine OrthoMAX Digital Photogrammetric System. *Photogrammetric Record* 16: 93, 519–531.

Griffey NJ & P Worsley (1978). The pattern of Neoglacial glacier variations in the Okstindan region of northern Norway during the last three millennia. *Boreas* 7, 1–17.

Gude M, G Daut, S Dietrich, R Mäusbacher, C Jonasson, A Bartsch & D Scherer (2002). Towards an integration of process measurements, archive analysis and modern geomorphology – the Kärkevagge experimental site, Abisko area, northern Sweden. *Geografiska Annaler A* 84, 205–212.

Gurney SD & DS Lawrence (2004). Seasonal trends in the stable isotopic composition of snow and meltwater runoff in a subarctic catchment at Okstindan, Norway. *Nordic Hydrology* 35, 119–137.

Hall KJ (1985). Some observations on ground temperatures and transport processes at a nivation site in northern Norway. *Norsk Geografisk Tidsskrift* 39, 27–37.

Harris C (1973). Some factors affecting the rates and processes of periglacial mass movements. *Geografiska Annaler A* 55, 24–28.

Harris C (1981). Microstructures in solifluction sediments from south Wales and north Norway. *Biuletyn Peryglacjalny* 28, 221–226.

Harris C (1982). The distribution and altitudinal zonation of periglacial landforms, Okstindan, Norway. *Zeitschrift für Geomorphologie* 26, 283–304.

Harris C (1986). Some observations concerning the morphology and sedimentology of a protalus rampart, Okstindan, Norway. *Earth Surface Processes and Landforms* 11, 673–676.

Harrison S & MG Macklin (1991). Form and size characteristics of clasts on stone-banked solifluction lobes, Okstindan, North Norway. *Norsk Geografisk Tidsskrift* 45, 155–160.

Holtedahl O (ed) (1960). Geology of Norway. *Norges Geologiske Undersøkelse* 208. 540 p.

King L (1986). Zonation and ecology of high mountain permafrost in Scandinavia. *Geografiska Annaler A* 68, 131–139.

Knudsen NT & N Haakensen (1998). Austre Okstindbre. In Kjøllmoen B (ed). *Glasiologiske Undersøkelser I Norge 1996 Og 1997*, 95–101. Norges vassdrags- og energiverk, Oslo.

Knudsen NT & WH Theakstone (1997). Recent changes of the glaciers of Svartisen and Okstindan, Norway. *Aarhus Geoscience* 7, 113–128.

Körner C (1999). *Alpine plant life: functional plant ecology of high mountain ecosystems*. 338 p. Springer, Berlin.

McCarroll D, RA Shakesby & JA Matthews (1998). Spatial and temporal patterns of late Holocene rockfall activity on a Norwegian talus slope: a lichenometric and simulation-modeling approach. *Arctic and Alpine Research* 30, 51–60.

Mugnier CJ (1999). Grids & Datums – the kingdom of Norway. *Photogrammetric Engineering & Remote Sensing* 65, 1129–1132.

Raben P, WH Theakstone & K Tørseth (2000). Relations between winter climate and ionic variations in a seven-meter-deep snowpack at Okstindan,

Norway. *Arctic, Antarctic and Alpine Research* 32, 189–196.

Rapp A (1960). Recent development of mountain slopes in Kärkevagge and surroundings. *Geografiska Annaler* 17, 71–200.

Reynolds JM (1978). The solid geology around Okstindsjøen. In Fenwick IM (ed). Okstindan Preliminary Report for 1976, Okstindan Research Project, 1–16. Unpublished report.

Rutland RWR & R Nicholson (1965). Tectonics of the Caledonides in part of Nordland, Norway. *Quarterly Journal of the Geological Society of London* 121, 73–109.

Shakesby RA (1997). Pronival (protalus) ramparts: a review of forms, processes, diagnostic criteria and palaeoenvironmental implications. *Progress in Physical Geography* 21, 394–418.

Strand T & O Kulling (1972). *Scandinavian Caledonides*. 302 p. Wiley, London.

Winkler S (2003). A new interpretation of the data of the 'Little Ice Age' glacier maximum at Svartisen and Okstindan, northern Norway. *The Holocene* 13, 83–95.

Worsley P (1993). Holocene solifluction at Okstindan, northern Norway: a reassessment. *Paläoklimaforschung* 11, 49–57.